Int J Adv Manuf Technol (2017) 91:1643–1659
DOI 10.1007/s00170-016-9873-9

ORIGINAL ARTICLE

Research of the Gurson damage model of the different yield functions during the deep-drawing process

Fan Xu[1,3] · **Jun Lin**[2] · **Shengdun Zhao**[3] · **Hao Zhang**[1]

Received: 21 September 2016 / Accepted: 7 December 2016 / Published online: 15 December 2016
© Springer-Verlag London 2016

Abstract Based on the macroscopic constitutive models (MCCM), the Gurson damage model is introduced to build the mesoscopic constitutive models (MSCM) with anisotropy Gurson-Hill1948 and Gurson-Yld2003 damage models. The damage parameters of the Gurson-Hill1948 and Gurson-Yld2003 damage models using orthogonal analysis and inverse computed methods are discussed and compared with experimental and simulation results obtained using the user subroutine VUMAT implemented by Lin. The corresponding sensitivity of the damage parameters was obtained by orthogonal analysis, then these optimized damage parameters could describe the mechanical performance for 08Al sheet with 1 mm thickness. Basically, the simulation results are in accordance with the experiment results. The damage parameters of the Gurson-Hill1948 and Gurson-Yld2003 constitutive models are explored to describe the deep-drawing deforming process, failure performance and obtained equivalent stress, equivalent plastic strain, thickness, damage distribution, and the influence of the friction coefficient during the deep-drawing process.

✉ Fan Xu
fan.xu@kuleuven.be

[1] Department of Materials Engineering, KU Leuven, Campus Gent, Gebroeders De Smetstraat 1, 9000 Ghent, Belgium

[2] No. 59 Institute of China Ordinance Industry, Yuzhou Road 33, Chongqing, China

[3] School of Mechanical Engineering, Xi'an Jiaotong University, Xi'an 710049, China

Keywords Deep drawing · Orthogonal analysis · Damage model · Constitutive model · Numerical analysis

1 Introduction

The demand for energy conservation has led the automotive industry to find new materials and plastic-forming methods to reduce the weight of vehicle body structures. Deep drawing is one of the mostly widely used forming processes to manufacture automotive body parts from sheet metal. Although the deep-drawing process is simple and popular in the industry, it produces cups at limited drawing ratios (not exceeding 2.2) because of the drawing resistance from the flange portion and the maximum tensile force at the wall of the semi-drawn cup. Many techniques have been adopted to achieve a higher drawing ratio as well as to increase production efficiency and obtain good-quality parts. To explore the new forming process of the metal sheets, a fundamental understanding of the forming limit of the sheet metal is necessary. At the same time, the characteristics of the metal sheet should be discussed. In order to increase the failure ratio, it is necessary to use FEA. The success of the simulation depends on the capacity of the constitutive models' respective material parameters to accurately reproduce the mechanical behavior.

During the deep-drawing process, it is easy to think the influence of the anisotropy on the simulation results. Many anisotropy yield models were proposed to describe the initial anisotropy and identified from the mechanical properties, such as Hill1848 [1], Barlat 2000 [2] yield models. Hill [1] proposed for the first time the anisotropy yield function, which was subsequently called the Hill1948 yield function. This

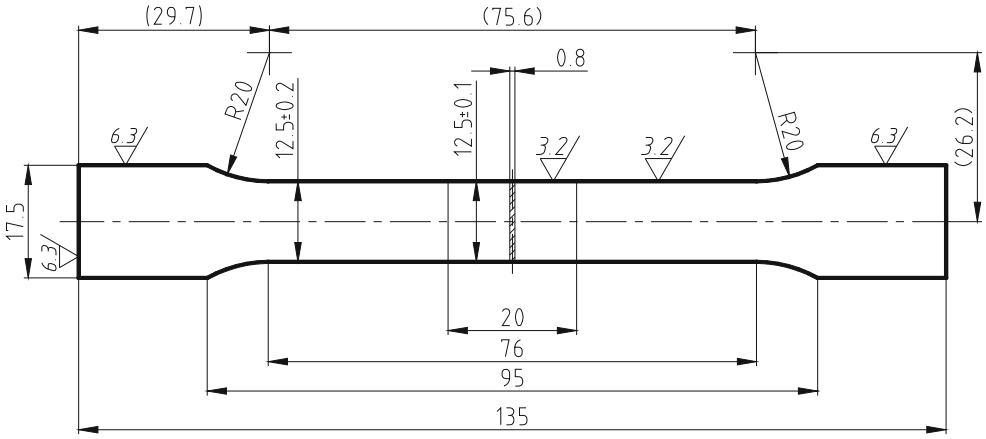

Fig. 1 The specimen for 08Al sheet with 1 mm thickness

yield function cannot accurately describe the anisotropy of the aluminum and copper alloys. To improve the predictive precision of the materials, R-Hill proposed several yield functions. Hill [3, 4] proposed two yield functions; this method belongs to the lower-order yield function.

$$\varphi(\sigma) = \sqrt{\frac{1}{2}\left(F(\sigma_{22})^2 + G(\sigma_{11})^2 + H(\sigma_{11}-\sigma_{22})^2 + N\sigma_{12}^2\right)} \tag{1}$$

Where $\sigma^T = (\sigma_{11}, \sigma_{22}, \sigma_{12})$/MPa;

F, G, H, and N are the parameters of the yield function.

This method is used to calculate the initial yield stresses Y_ϕ and Y_b, also the stress-based method, and it can be written as shown in the following equations:

$$F = \left(-1 + \chi_{90}^2 + \chi_b^2\right), G = \left(1-\chi_{90}^2 + \chi_b^2\right), H = \left(1 + \chi_{90}^2-\chi_b^2\right), N = \left(4\chi_{45}^2-\chi_b^2\right) \tag{2}$$

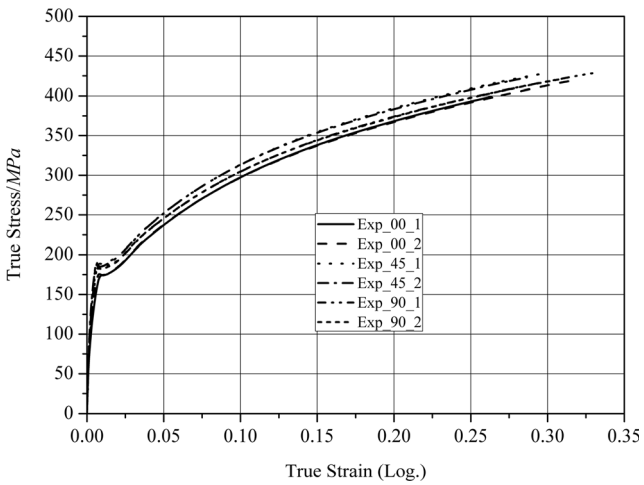

Fig. 2 The true stress-true strain under uniaxial tension

$$\chi_a = Y_0/Y_a, \chi_b = Y_0/Y_b \tag{3}$$

$$\chi_b = (\chi_0 + 2\chi_{45} + \chi_{90})/4 \tag{4}$$

The $\phi = (0, 45, 90)$ is the orientation angle of the tensile test specimen's longitudinal axis relative to the original rolling direction. Y_ϕ is the initial yield uniaxial stress with the same testing method.

Barlat proposed some anisotropy yield functions [2, 5] that were widely applied in simulating the plastic-deformation process; these functions belong to the higher-yield functions. They took a yield function to describe the behavior of sheet metals exhibiting planar anisotropy and subjected to plane stress conditions. It can approximate plastic potential calculated with the Taylor/Bishop and Hill theory of polycrystalline plasticity for stress states. Aretz [6] thought that anisotropy influences the major stress; he proposed Yld2003 yield function and used this function in the damage model. He changed Hosford's [7] yield function as the following equation:

$$\varphi(\sigma) = \sqrt[m]{\frac{1}{2}\left(\left|\sigma_2^{'}\right|^m + \left|\sigma_1^{'}\right|^m + \left|\sigma_1^{''}-\sigma_2^{''}\right|^m\right)} \tag{5}$$

Where

$$\left.\begin{matrix}\sigma_1^{'} \\ \sigma_2^{'}\end{matrix}\right\} = \frac{a_1\sigma_{11} + a_2\sigma_{22}}{2} \pm \sqrt{\left\{\frac{a_3\sigma_{11}-a_4\sigma_{22}}{2}\right\}^2 + a_5\sigma_{12}} \tag{6}$$

Table 1 Isotropic hardening equation parameters for the 08Al sheet

Direction (deg)	No.	Yield stress (MPa)	$\bar{\varepsilon}_0$	Hardening index n	Enhancement factor K (MPa)
0	I	170	0.016	0.281	586.7
	II	171	0.016	0.277	579.7
45	I	184	0.016	0.271	589.8
	II	181	0.015	0.271	588.7
90	I	181	0.017	0.271	575.6
	II	175	0.015	0.275	576.1

Table 2 The mechanical performance for the 08Al sheet

Direction	Young module	Poisson's ratio	χ value	R value
0	197	0.28	1.0000	1.66
45			1.0704	1.38
90			1.0440	2.19
EB			1.0462	1.65

$$\left.\begin{matrix}\sigma_1'' \\ \sigma_2''\end{matrix}\right\} = \frac{\sigma_{11}+\sigma_{22}}{2} \pm \sqrt{\left\{\frac{a_6\sigma_{11}-a_7\sigma_{22}}{2}\right\}^2 + a_8\sigma_{12}} \tag{7}$$

$a_1, \ldots, a_8$ are parameters of material.

The yield function considered in this subsection is frequently called "Yld2003-2d" and was developed [5, 8]. The previous literature shows the influence of anisotropy on deformation process. At the same time, some additional phenomenon will also be discussed by using the different constitutive equations. Shang et al. [9] focused on the development of pore shape anisotropy during sintering forging. They investigated the evolution of pore anisotropy and grain growth in hierarchical porous ceramics during sinter forging. There is a clear difference between the preferential orientation of the extrinsic and intrinsic pores. Xue et al. [10] used the Yld2000 [2] and Hill1948 [1] yield functions to create the constitutive equation. At the same time, they tried to use a method to calibrate the parameters of the constitutive equations. Bandyopadhyay et al. [11] discussed that finite element simulations were conducted using the Barlat-89 [5] and Hill1948 [1] anisotropy yield criteria coupled with theoretical FLD to evaluate LDR and deep-drawing behavior of three parent materials and two TWBs of DP steels. Taherizadeh et al. [12] compared three models for simulation forming of anisotropy sheet metals containing a non-AFR with both yield and potential functions in the Hill form with different calibration, an AFR with a non-quadratic yield function of Yld2000 [2], a non-AFR non-quadratic yield function of Yld91 [13], and plastic potential function of Yld89 [5]. Safaei et al. [14] presented a plane stress anisotropy constitutive model with mixed isotropic–kinematic hardening. Quadratic Hill1948 and non-quadratic Yld2000-2d yield criteria were considered in a non-AFR model to account for anisotropy behavior. Moayyedian and Kadkhodayan [15] introduced a modified Yld2000-2d II inserting the modified Yld2000-2d and Yld2000-2d in place of yield and plastic potential functions, respectively, to model anisotropy pressure-sensitive sheet metals.

Table 3 The parameters of Yld2003 function

m	α_1	α_2	α_3	α_4	α_5	α_6	α_7	α_8
6	0.9427	1.1133	0.9454	0.7693	1.2705	1.0436	1.1123	0.9384

Basically, ductile failure in metals occurs because of the nucleation, growth, and coalescence of voids [16, 17]. Voids are nucleated in metals mainly by decohesion at the particle–matrix interfaces or by micro-cracking of second-phase particles (see, for example, Tvergaard [18]). Additionally, voids nucleate in single crystals that contain neither pre-existing voids nor inclusions. Thus, the ability to accurately describe the evolution of voids in a ductile metal is necessary to accurately predict its failure. Deep-drawing steel is considered a porous media. Guo et al. [19] explored a modified Rousselier model and introduced a calibration procedure of the damage parameters. This model describes the evolution of the fracture by using the initial void volume fraction and the shear damage parameter. In this paper, the void theory is used to explain the failure process. Xu et al. [20] used a modified Gurson-Tvergaard-Needleman (GTN) damage parameter to explore the clinching process and the failure mechanism and to describe the evolution of the failure. The Gurson model has been proposed to describe plastic deformation for such types of materials. This model has attracted significant attention, and various modifications have been proposed. Lin [8] implemented the Hill1948 [1] and Yld2003 [6] yield functions to build macro-constitutive equations. However, their disadvantage is that they cannot describe the sudden force decline using the macro-constitutive equation. The Gurson damage model was widely applied in simulating the deformation of the material. In the work of Malte et al. [21], an explicit finite element model of the deep drawing of a paperboard was developed by using a custom yet simple material model that describes the anisotropy and plasticity of paperboard. This model was found to predict the experimental results with reasonable accuracy up to the point when wrinkling began to dominate the material response. Lin et al. [22] showed that a new type of passive-pressurized hydro-mechanical deep-drawing (PHDD) tool with two pistons was designed and manufactured. Further analysis shows that the design of the new tool is reasonable and the hydraulic pressure used in all experiments is in good agreement with the analytical results using ABAQUS/Explicit subroutine. Lin et al. [23] proposed a maximum shear stress-calculating method called shear failure criterion. This approach used the advanced constitutive models, including the Hill1948 [1] and Yld2000-2d [2] yield functions and several types of isotropic hardening models.

The present study used Lin's model to calibrate the constitutive equations and discuss the parameters of the deep-drawing process. Section 2 introduces these constitutive equations. At the same time, the parameters of these constitutive equations are calibrated by using orthogonal analysis and inverse computing. According to this result, it shows how many factors affected the force and the displacement, and then the optimization damage parameters will be obtained. Section 3

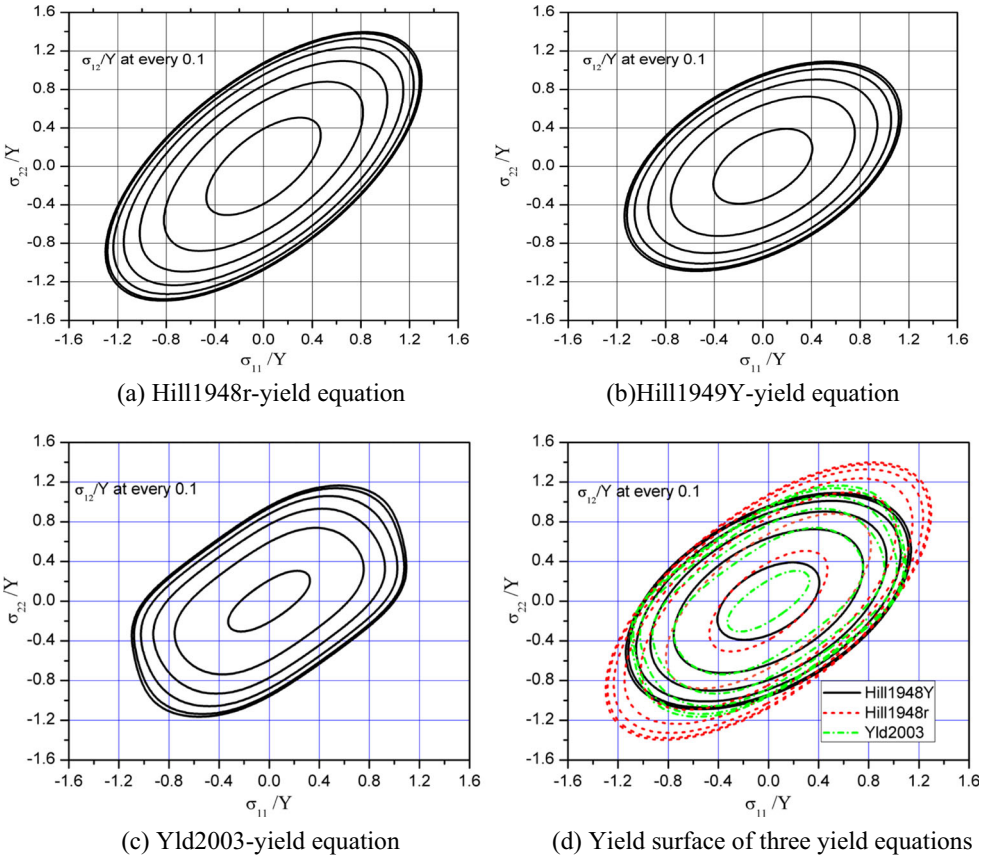

(a) Hill1948r-yield equation (b)Hill1949Y-yield equation

(c) Yld2003-yield equation (d) Yield surface of three yield equations

Fig. 3 The yield locus of the different constitutive equations for the 08Al sheets. **a** Hill1948r-yield equations. **b** Hill1949Y-yield equation. **c** Yld2003-yield equation. **d** Yield surface of three yield equations

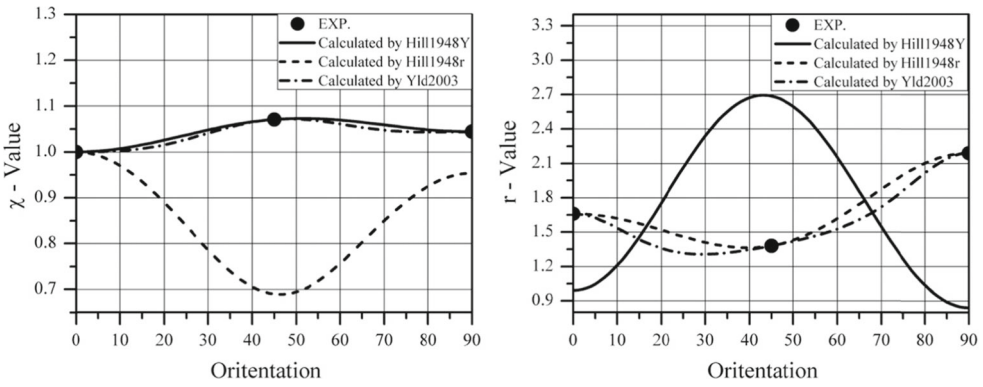

(a) The initial yield strress ratio (b) R-values

Fig. 4 Comparison between predictive results and the experiment results. **a** The initial yield stress ratio. **b** *R* values

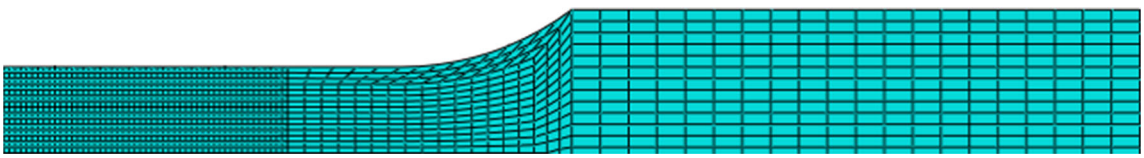

Fig. 5 2D FE model

Table 4 The parameters and the levels

Level	q_1	q_2	f_0 (A)	S_N	f_N (B)	ε_N (C)	f_c (D)	κ	K (E)	n (F)
1	1.539	1.794	0.0001	0.1	0.030	0.6	0.03	10	550	0.259
2	1.539	1.794	0.0005	0.1	0.035	0.65	0.04	10	560	0.269
3	1.539	1.794	0.0008	0.1	0.040	0.70	0.05	10	570	0.279
4	1.539	1.794	0.001	0.1	0.045	0.75	0.06	10	580	0.289
5	1.539	1.794	0.008	0.1	0.050	0.8	0.07	10	590	0.299

Table 5 The results of orthogonal design

	A	B	C	D	E	F	Force	Gap force	Displacement	Gap displacement
1	1	1	1	1	1	1	3875.5036	125.0636	40.071	3.639
2	1	2	2	2	2	2	3302.75	447.69	36.577	0.145
3	1	3	3	3	3	3	3550.1231	200.3169	35.127	1.305
4	1	4	4	4	4	4	3500.1023	250.3377	34.775	1.657
5	1	5	5	5	5	5	3400.75	349.69	35.114	1.318
6	2	1	2	3	4	5	3245.7756	504.6644	35.662	0.77
7	2	2	3	4	5	1	3879.1253	128.6853	38.7705	2.3385
8	2	3	4	5	1	2	3750.1103	0.3297	38.113	1.681
9	2	4	5	1	2	3	3465.7791	284.6609	36.552	0.12
10	2	5	1	2	3	4	3795.1102	44.6702	36.747	0.315
11	3	1	3	5	2	4	3575.2013	175.2387	36.723	0.291
12	3	2	4	1	3	5	3775.1209	24.6809	38.553	2.121
13	3	3	5	2	4	1	3674.8931	75.5469	38.554	2.122
14	3	4	1	3	5	2	3679.1542	71.2858	36.221	0.211
15	3	5	2	4	1	3	3877.2143	126.7743	37.551	1.119
16	4	1	4	2	5	3	3751.2371	0.7971	36.773	0.341
17	4	2	5	3	1	4	3681.5102	68.9298	36.779	0.347
18	4	3	1	4	2	5	3451.2307	299.2093	37.11	0.678
19	4	4	2	5	3	1	3840.1631	89.7231	38.992	2.56
20	4	5	3	1	4	2	3514.0942	236.3458	35.777	0.655
21	5	1	5	4	3	2	3575.1261	175.3139	33.691	2.741
22	5	2	1	5	4	3	3591.234	159.206	36.759	0.327
23	5	3	2	1	5	4	3423.5697	326.8703	35.972	0.46
24	5	4	3	2	1	5	3555.3289	195.1111	35.275	1.157
25	5	5	4	3	2	1	3689.1524	61.2876	34.965	1.467

Table 6 Extreme difference analysis (force)

	A	B	C	D	E	F
K1	17,629.229	18,022.84	18,392.23	18,054.07	18,739.67	18,958.84
K2	18,135.9005	18,229.74	17,689.47	18,079.32	17,484.11	17,821.23
K3	18,581.5838	17,849.93	18,073.87	17,845.72	18,535.64	18,235.59
K4	18,238.2353	18,040.53	18,465.72	18,282.8	17,526.1	17,975.49
K5	17,834.4111	18,276.32	17,798.06	18,157.46	18,133.84	17,428.21
k1	3525.8458	3604.569	3678.447	3610.814	3747.933	3791.768
k2	3627.1801	3645.948	3537.895	3615.864	3496.823	3564.247
k3	3716.31676	3569.985	3614.775	3569.143	3707.129	3647.118
k4	3647.64706	3608.106	3693.145	3656.56	3505.22	3595.099
k5	3566.88222	3655.264	3559.612	3631.492	3626.767	3485.641
R1	190.471	85.27884	155.2501	87.41664	251.1108	306.1263
Rank	3	6	4	5	2	1

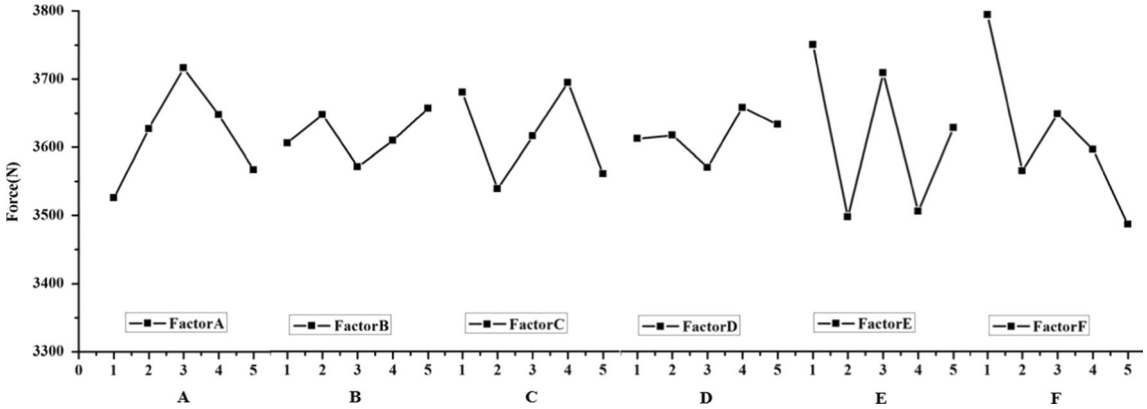

Fig. 6 Effect of process parameters on the strength of the sheet for 08Al

compared the simulation results with the experiment results to explore the change of some important parameters.

2 Calibration of constitutive equation

The different macro-constitutive equations have different precise simulations. The macro-constitutive equation based on the second-order Hill1948 [1] yield function describes the initial yield stress and the *R* value. To improve the precision of the macro-constitutive equation, this paper introduces the higher-order Yld2003 [6] yield function that describes the initial yield stress and *R* value. On the basis of the two macro-constitutive equations, it combined with the Gurson damage model to build the micro-constitutive equation to predict the sudden force decline after sheet instability. Selecting a suitable yield function to improve constitutive model precision is an important task. In this paper, Hill1948 [1] and Yld2003 [6] yield functions were used. At the same time, two yield functions were combined with the Gurson damage model to build two micro-constitutive equations. Basically, the constitutive equation of the material included the elastic–plastic macro-constitutive model, isotropic hardening model, plane anisotropy yield equation, and damage model.

Table 7 Extreme difference analysis (displacement)

	A	B	C	D	E	F
*K*1	181.664	182.92	186.908	186.925	187.789	191.3525
*K*2	185.8445	187.4385	184.754	183.926	181.927	180.379
*K*3	187.602	184.876	181.6725	178.754	183.11	182.762
*K*4	185.431	181.815	183.179	181.8975	181.527	180.996
*K*5	176.662	180.154	180.69	185.701	182.8505	181.714
*k*1	36.3328	36.584	37.3816	37.385	37.5578	38.2705
*k*2	37.1689	37.4877	36.9508	36.7852	36.3854	36.0758
*k*3	37.5204	36.9752	36.3345	35.7508	36.622	36.5524
*k*4	37.0862	36.363	36.6358	36.3795	36.3054	36.1992
*k*5	35.3324	36.0308	36.138	37.1402	36.5701	36.3428
R^2	2.188	1.4569	1.2436	1.6342	1.2524	2.1947
Rank	2	4	6	3	5	1

2.1 Calibration of macro-constitutive model

The material parameters of the constitutive models were identified from the mechanical test data. The experimental stress–strain curves were obtained from uniaxial tension tests in three different directions (0°, 45°, and 90° with respect to RD). The material used in this study is 08Al sheet. The initial specimen size is shown in Fig. 1. The specimens with the geometry were cut according to the different rolling directions. At the same time, quasi-static tests were conducted at room temperature using a 20-kN Instron universal testing machine.

Figure 2 shows the true stress and true strain curve under uniaxial tension for the different rolled directions where anisotropy is shown. In this paper, the influence of anisotropy is discussed. A standard value of $E = 197{,}000$ MPa was applied for Young's modulus based on the assumption that plastic incompressibility, true stress, and true strain were determined from the nominal stress and strain with the well-known relations $\varepsilon = \ln(1+e)$ and $\sigma = s(1+e)$, while plastic strain was calculated as $\varepsilon^p = \varepsilon - \sigma/E$. True stress and plastic strain were from ABAQUS. Isotropic hardening equation parameters for 08Al sheet are shown in Table 1. The segment functions were used to represent each individual true stress plastic strain curve.

$$Y = \begin{cases} Y_0 & \left(0 \le \bar{\varepsilon}^{\mathrm{p}} \le \bar{\varepsilon}_0\right) \\ K \cdot \left(\bar{\varepsilon}^{\mathrm{p}}\right)^n & \left(\bar{\varepsilon}_0 \le \bar{\varepsilon}^{\mathrm{p}}\right) \end{cases} \tag{8}$$

The previous papers discussed some constitutive models to describe the performance of the materials. Normally, a

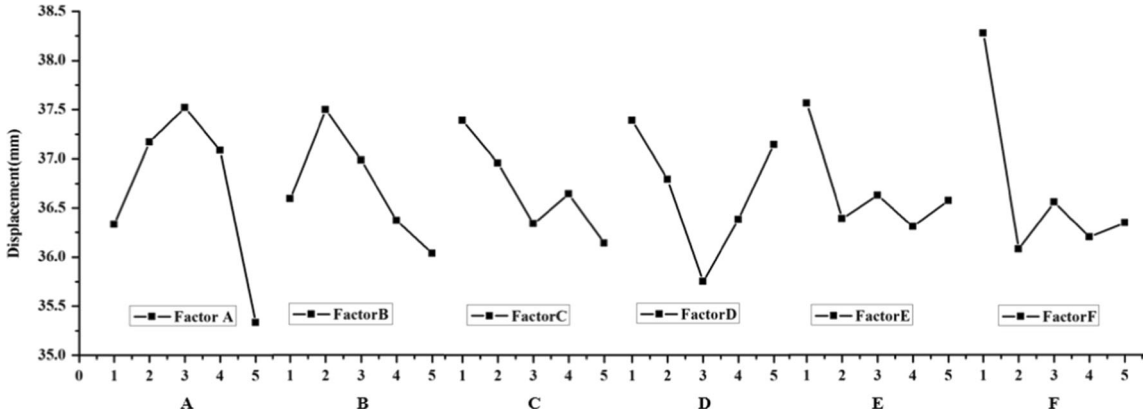

Fig. 7 Effect of process parameters on displacement during the tensile test

constitutive model comprises hardening behavior, damage model, flow behavior, and yield function. So in this paper, Hill1948 yield function and Yld2003 yield function were discussed to get the macroscopic constitutive models (MCCM) and the mesoscopic constitutive models (MSCM).

2.2 Yield functions

The anisotropy parameters for the rolled 08Al sheet are reported in Table 2. The mechanical behavior anisotropy demonstrated a significant improvement in changing the rolling route. Table 3 shows the parameters of the Yld2003 function obtained by using the LM algorithm.

2.2.1 The evaluation of all yield functions

Figure 3 shows the comparison for Hill1948Y, 1948r, and Yld2003 with regard to yield shape. Figure 3a–c shows that the yield surfaces of Hill1948Y and Hill1948r are close to the ellipse, while the yield surface of Yld2003 is not. A larger difference exists between using the initial yield stress ratio and the thick anisotropy to determine yield locus; the yield surface of Hill1948Y is close to that of Yld2003 as shown in Fig. 3d. At the same time, no obvious change occurs for Hill1948 yield locus with the increase in shear stress σ_{12}, but change happened in the Yld2003 yield locus.

The predictive value was compared with the experimental value for the initial yield stress ratio and R value of Hill1948Y, Hill1948r, and Yld2003, respectively, as shown in Fig. 4. Figure 4 shows that for the Hill1948Y function, the predictive stress value is in accordance with the experimental value when the initial yield stress ratio ensures the yield function. For Hill1948r yield function, the yield function based on the R value accurately predicts the R value, but great difference occurs in predicting stress. For the Yld2003 yield function, the yield function accurately predicts not only the R value but also stress. According to Fig. 4a, the Hill1948Y and Yld2003 yield functions obtain the same predictive values. The Hill1948r and Yld2003 yield functions are in accordance with the experimental point, but some differences in the other regions are shown in Fig. 4b. The best reason is that Hill1948r

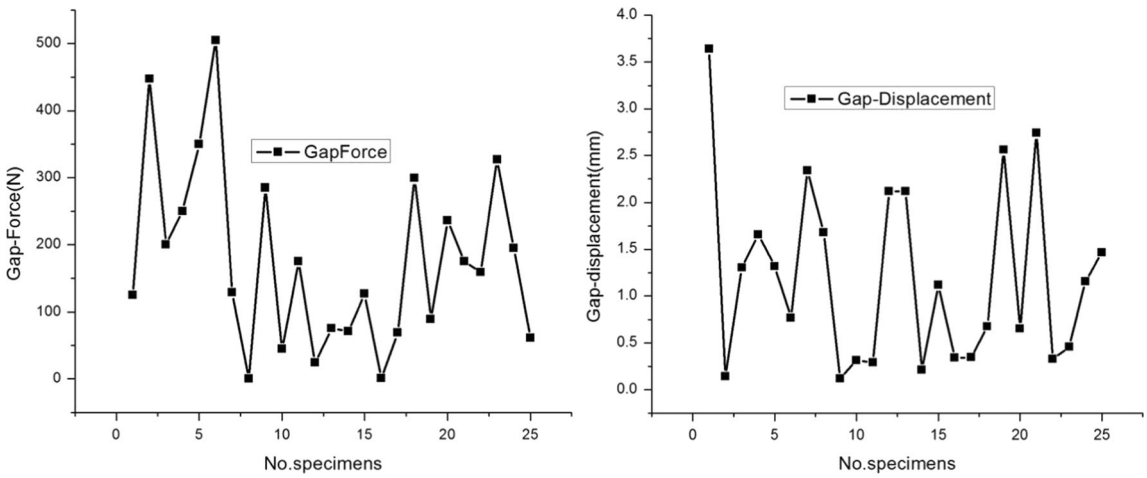

Fig. 8 The gap displacement and gap force

Table 8 The optimized the parameters for the 08Al

	A	B	C	D	E	F
G-Hill1948	4	1	4	2	5	3

is a second-order yield function but Yld2003 yield function is a high-order yield function (m = 6). This paper uses the Hill1948 yield function to represent Hill1948r.

2.3 Calibration of the mesoscopic constitutive models

At present, the damage parameters and the index of the hardening behavior is dependent on FE for comparison simulation results with the experimental results. Basically, the trial-and-error method is an important method to obtain these parameters; however, the orthogonal analysis is discussed in this paper to get the damage parameters and the index of the hardening behavior.

The sensitivity of the damage parameters is explored as follows. Figure 5 shows the 2D model. On the basis of the symmetry, a 1/4 model was used. To accurately describe the tensile process, the displacement was assumed to be 50 mm.

If Swift equation is regarded as hardening behavior, these parameters (K, n) need to be ensured. At the same time, these parameters ($f_0, f_N, \bar{\varepsilon}_N$, and f_c) are calibrated. f_0 and S_N are the natural performance of the materials. For low-carbon steel, $(f_0, S_N) = (0.001, 0.1)$. In this paper, an orthogonal analysis method is proposed to arrange simulation time and assess results.

2.4 Orthogonal design

After ensuring the sensitivity of the damage parameters, to reduce validity time and evaluate a group-suitable damage parameter, a specially designed analysis procedure is needed. Wen et al. [24] presented a response surface optimization of the clinching tools. The Taguchi method is a powerful and is the most commonly used technique for experiment design. Thus, in the following sections, FE simulation and orthogonal design were used to identify the damage parameters of the Gurson-Yld2003 and Gurson-Hill1948 damage models in terms of tensile force and displacement.

Table 9 The mechanical performance of the MSCM for 08Al

Damage model	E (GPa)	v	k	K	n	$\bar{\varepsilon}_0$
Gurson-Hill1948	197,000	0.28	400	584.9	0.281	0.016
Gurson-Yld2003			400	591.9	0.289	0.016

Table 10 The damage parameters of the MSCM for the 08Al

Damage model	q_1	q_2	f_0	S_N	f_N	ε_N	f_c	κ
Gurson-Hill1948	1.539	1.794	0.001	0.1	0.035	0.75	0.041	10
Gurson-Yld2003	1.539	1.794	0.001	0.1	0.030	0.82	0.0375	10

Based on a comprehensive view of FEM analysis and relative references, the key damage parameters of Gurson-Yld2003 and Gurson-Hill1948 in orthogonal design include the initial void volume fraction (f_0), void volume fraction at nuclear (f_N), mean (ε_N), critical void volume fraction (f_c), hardening coefficient (K), and enhancement factor (n), and other parameters that are fixed [8]. An orthogonal array table is expressed as $L_{25}(5^6)$ with an establishment of six 5-level factors as presented in Tables 4 and 5.

Extreme difference analysis (Table 6) for the maximum force was introduced to find out how much the factors affect the maximum force. Table 6 is the result of analysis, and Fig. 6 shows the effect curves of the factors. It is obvious that n is the most important factor that influences the maximum force.

Extreme difference analysis (Table 7) for the maximum displacement was introduced to find out how much factor affect the maximum displacement. Table 7 is the result of analysis, and Fig. 7 shows the affected curves of the factors. Apparently, n is the most important factor that influences the displacement. At the same time, it can be found that the initial void volume fraction n is also an important factor that influences the displacement.

According to these conclusions, we select a group of parameters that came from 25 time simulation results as a group of optimized parameters, since the maximum force and the maximum displacement cannot valuate which parameters are right to describe the performance of the 08Al sheet. Figure 8 shows the min-gap force, which means that the force from the simulation is close to the experiment results. At the same time, the min-displacement from simulation is close to the experiment results. It is easy to find that the gap force and the displacement of the 16 specimens are close to the experiment results. According to the above analysis, Table 8 was obtained.

Table 11 The contact state during the deep drawing

Contact	Main surface	Slave surface	Friction coefficient
Interaction-punch	Punch	Blank	0.13
Interaction-die	Die	Blank	0.10
Interaction-blank holder	Blank holder	Blank	0.10

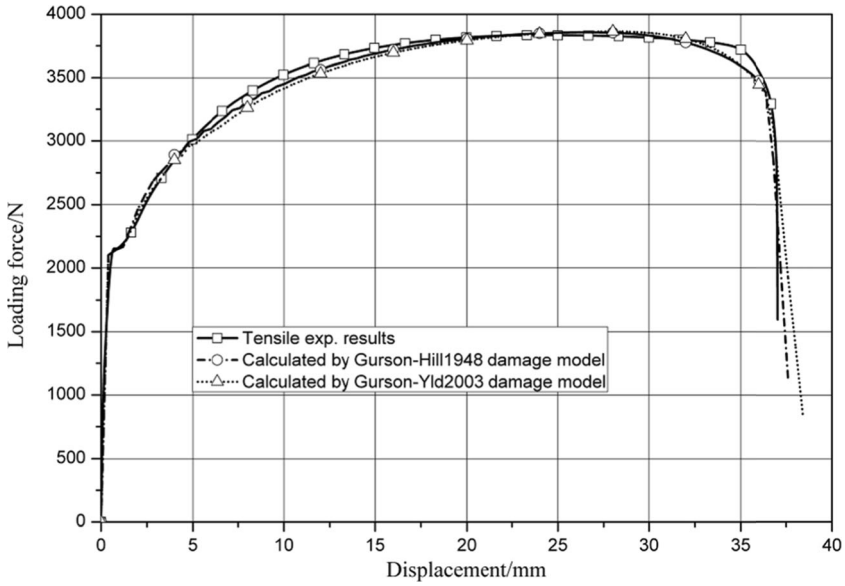

Fig. 9 Comparison between the damage models and the experiment

Table 8 shows the optimized parameters for the 08Al using the Gurson-Hill1948 damage model. There are some differences between the experiment and the simulation by using Gurson-Hill1948 damage model, so it is necessary to re-optimize the performance parameters and the damage parameters. Analysis shows how many factors affected the force and the displacement. The second optimization results are shown in Tables 9 and 10. The experimental result is in accordance with the simulation result using the Gurson-Hill1948 damage parameters as shown in Fig. 9. The same method was used to get the parameters of the Gurson-Yld2003, so the detailed procedure will not be shown in this paper.

Based on the above discussion, the damage parameters of Gurson-Yld2003 and Gurson-Hill1948 are obtained as shown in Table 9 (mechanical performance of the MSCM for 08Al sheet) and Table 10 (damage parameters of the MSCM for 08Al sheet). These parameters were used to describe the uniaxial tensile process. Basically, the simulation results are in accordance with the experimental results. Figure 9 shows that the Gurson damage model including Gurson-Yld2003 damage model and Gurson-Hill1948 damage model can accurately describe the tensile process. So, in the following discussion, these damage parameters will be used to describe the deep-drawing process.

3 Results and discussion

According to the second section, the MSCM including Gurson-Hill1948 and Gurson-Yld2003 damage models was

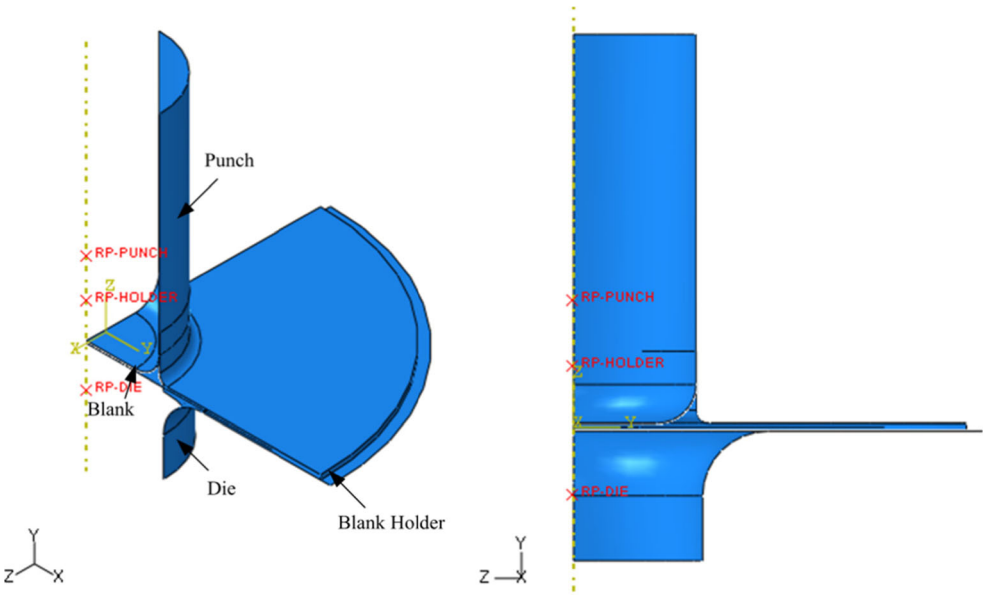

Fig. 10 3D model of deep-drawing specimen

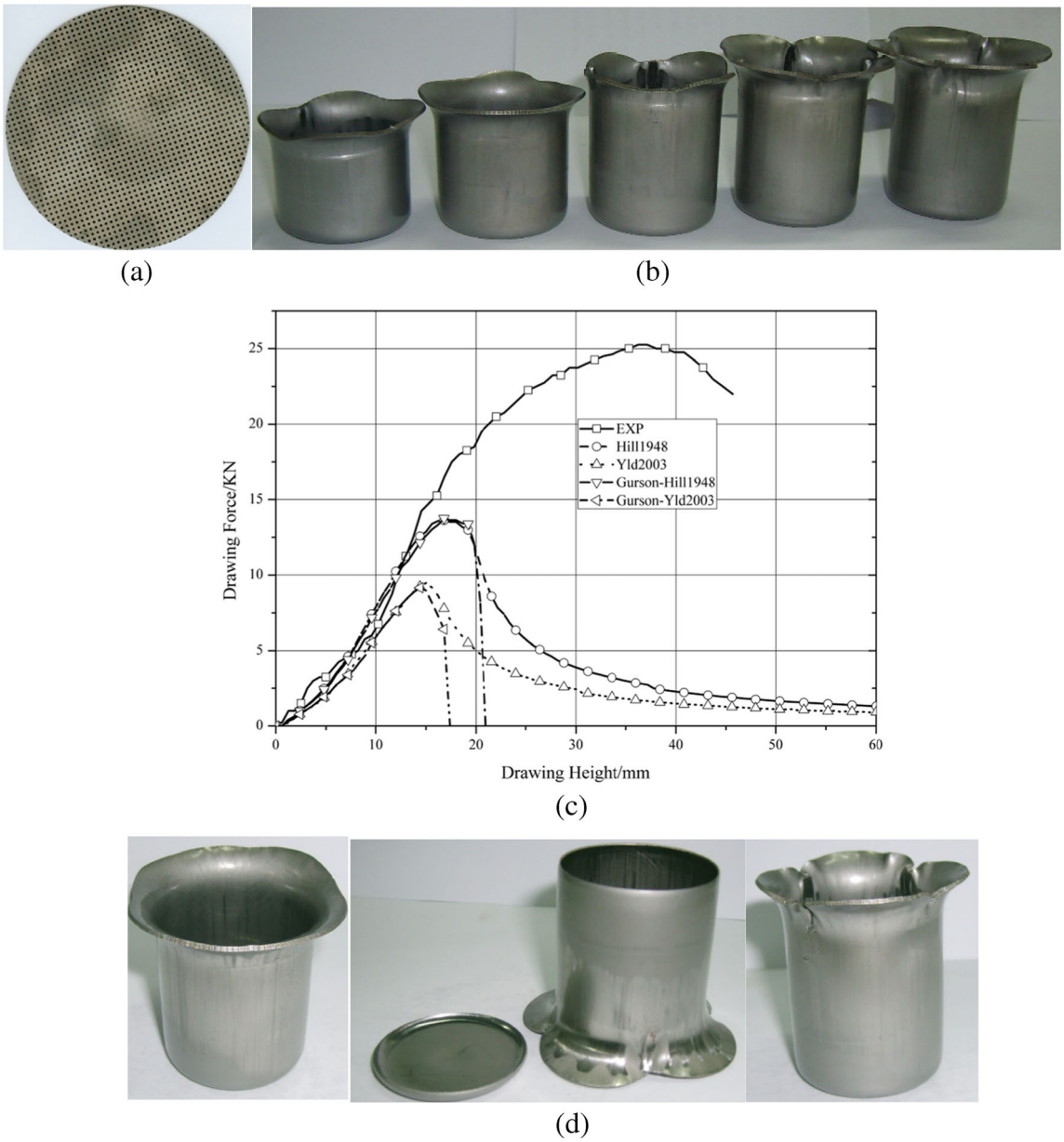

Fig. 11 Experiment results and simulation results. **a** Blank. **b** The different diameters (80, 85, 90, 95, and 98). **c** The drawing force and drawing height curve (1/4 mode). **d** Diameter 95 with qualified and failure samples

used to study the deep-drawing deformation process. During the deep-drawing deformation process, some factors and parameters will be discussed. In metal–plastic simulation, determining suitable contact state plays an important role in the deformation process. Figure 10 shows that the 3D model of the deep-drawing specimen have three contact surfaces, including the contact surface between the punch and the sheet (interaction-punch), the contact surface between the blank holder and the sheet (interaction-holder), and the contact surface between the die and the sheet (interaction-die).

In ABAQUS, the main and slave surfaces must be considered. The friction coefficient is an important parameter that influences the simulation results. The sheet bears a slight normal force during the deep-drawing process, so the Coulomb friction model was used. Rigid shell elements are utilized to model the tools: die, punch, and blank holder. The contacts between blank–die, blank–punch, and blank–blank holder are modeled as surface to surface. Karupannasamy et al. [25] showed a growing interest in developing contact models to predict the nature of friction conditions for use in FE calculations. A model is implemented to describe the friction behavior and deformation of surfaces for loading. The model has been compared with data from experiments using a rotational friction tester under multiple loading conditions. Zhang et al.

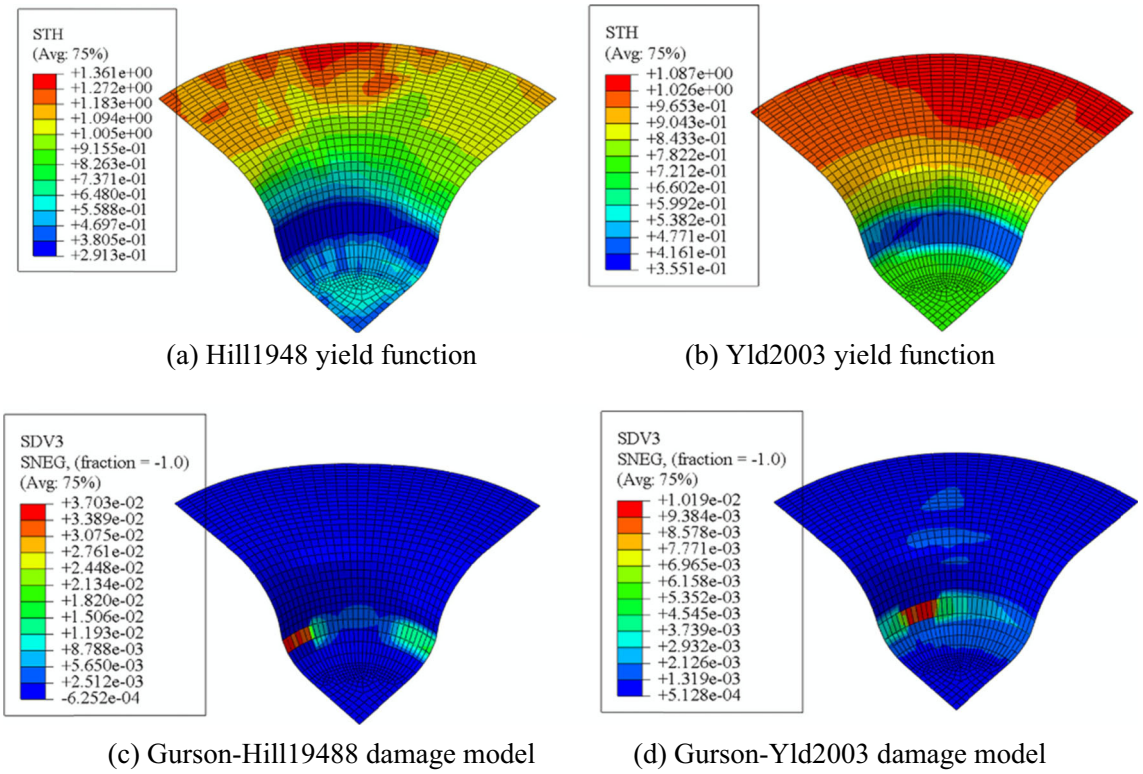

Fig. 12 The key failure parameter distribution on the sheet on the uniform deformation and inhomogeneous deformation (STH express thickness and SDV3 express damage parameters). **a** Hill1948 yield function. **b** Yld2003 yield function. **c** Gurson-Hill1948 damage model. **d** Gurson-Yld2003 damage model

[26] show that the friction coefficient between the sheet and the tools is close to 0.15–0.20. Table 11 shows the contact state during the deep drawing.

When the MCCM is used, the failure mode is described on the basis of the thickness change. When the MSCM is used, the failure mode is described according to the void volume fraction f. This 3D model is similar to the experiment except that the external surface of the sheet and the margin is without any hydraulic pressure. During the deep-drawing process, five size cups will be obtained. The maximum drawing ratio for the 08Al sheet is not more than 2.6. During drawing experiment, it has a great significance to deform the diameter of the blank being 80, 85, 90, 95, and 98 mm. In this paper, the 95-mm diameter sample is regarded as subject to research. In this experiment, a series of experiments are performed for 1.0 mm thickness 08Al sheet with different diameters using the new-type HDD process tooling on the XP-S-500 universal hydraulic system [8].

Figure 11 shows the comparison between the simulation results and the experiment for drawing force and drawing height using different constitutive equations including Hill1948, Yld2003, Gurson-Hill1948, and Gurson-Yld2003. Figure 11a shows a blank. Figure 11b shows the different diameter samples (80, 85, 90, 95, and 98 mm), but the 95-mm diameter sample is regarded as a simulation model to be discussed. As shown in Fig. 11c, the sheet with a 95-mm diameter was broken near $\pi/2$ of the plastic-coat corner at the filet corner of the die during deep drawing. At the same time, the drawing force of the MCCM and the MSCM using the same yield function are close before the failure. Although the parameters of the isotropic hardening equations of the MCCM and the MSCM are not the same, their predictive values are the same. When the MCCM is used, the drawing force changes with the changing of the height, but it cannot describe the decline phenomenon of the drawing force when the crack happened. When the MSCM is used, the decline phenomenon of the drawing force is described when the sheet is broken. A larger difference is observed between the predictive and the experimental results when using the different yield functions of the MCCM and the MSCM. Figure 11d shows the good and failed samples with the failure phenomenon at the bottom and the flange.

The distribution of the key failure parameters on the sheet of the uniform and inhomogeneous deformations at some point are shown in Fig. 12. STH (thickness) is an important parameter describing the failure process during the simulation process using the MCCM as shown in Fig. 12a, b. The other damage parameter, SDV3 (f), also describes the failure process during the deep-drawing process as shown in Fig. 12c, d. If the MCCM is used,

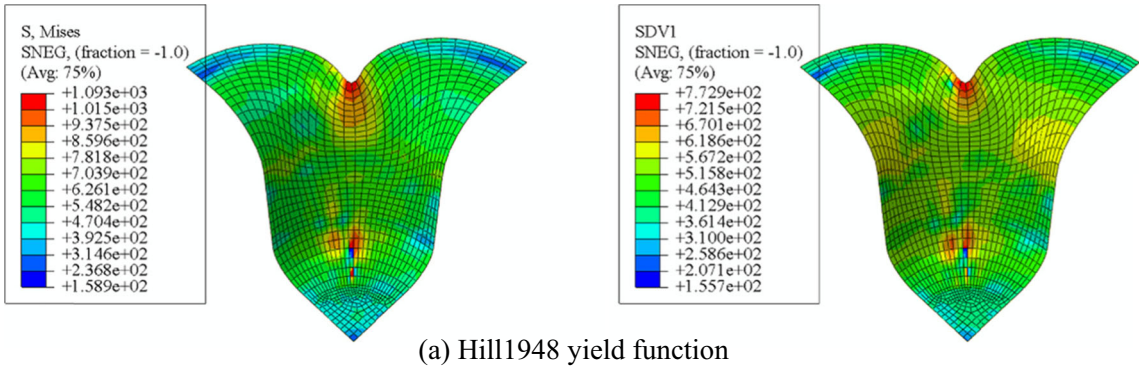

(a) Hill1948 yield function

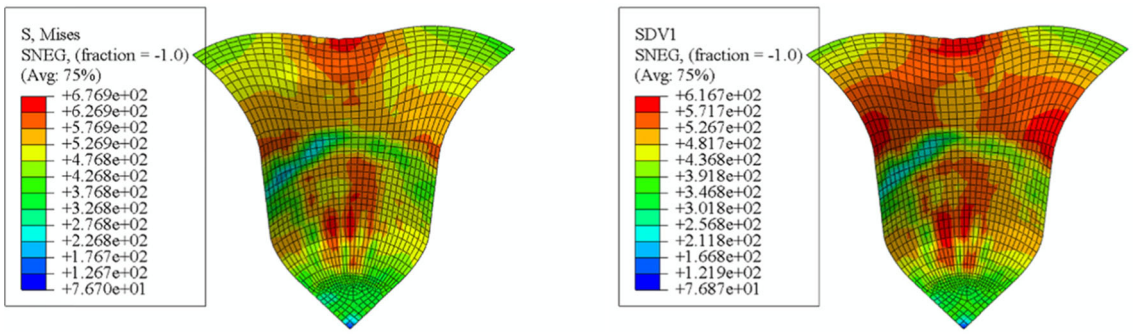

(b) Yld2003 yield function

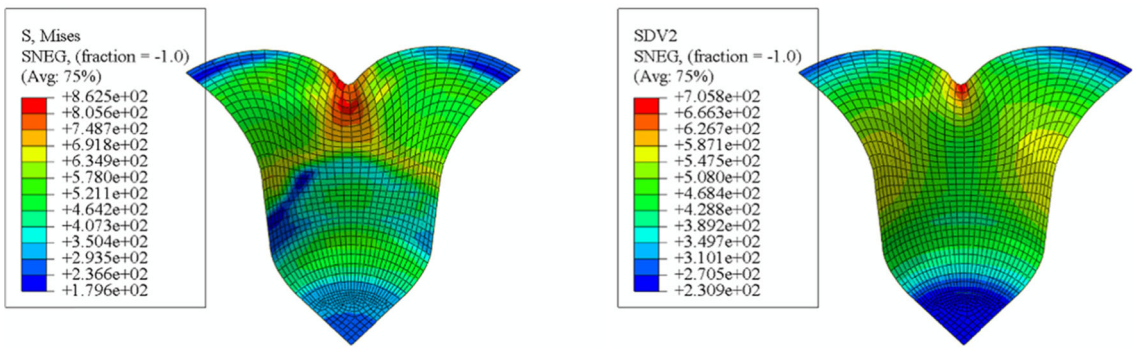

(c) Gurson-Hill1948 damage model

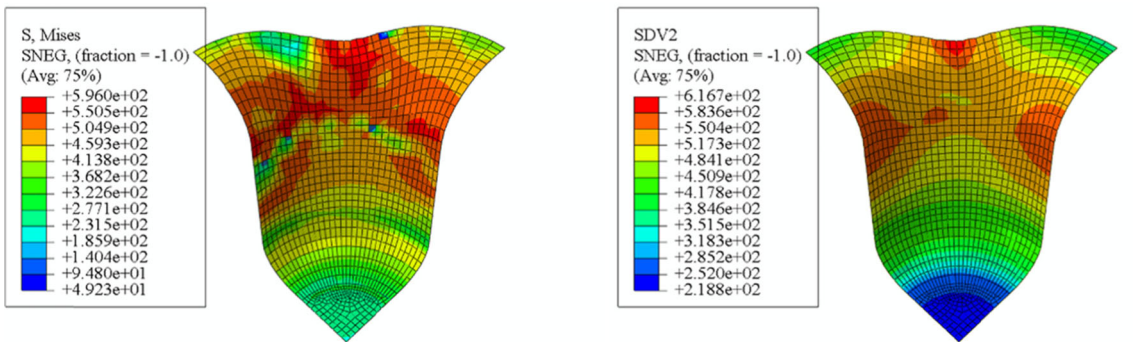

(d) Gurson-Yld2003 damage model

Fig. 13 The equivalent stress of Mises and the constitutive model during the mechanical-hydraulical assistance. **a** Hill1948 yield function. **b** Yld2003 yield function. **c** Gurson-Hill1948 damage model. **d** Gurson-Yld2003 damage model

it cannot describe the stage when the drawing force is suddenly equal to 0 but can describe the gradual decline process. Indeed, this result does not meet the actual situation. In the MSCM, the damage parameter is important in describing the deep-drawing process because it can describe the sudden change of force to 0.

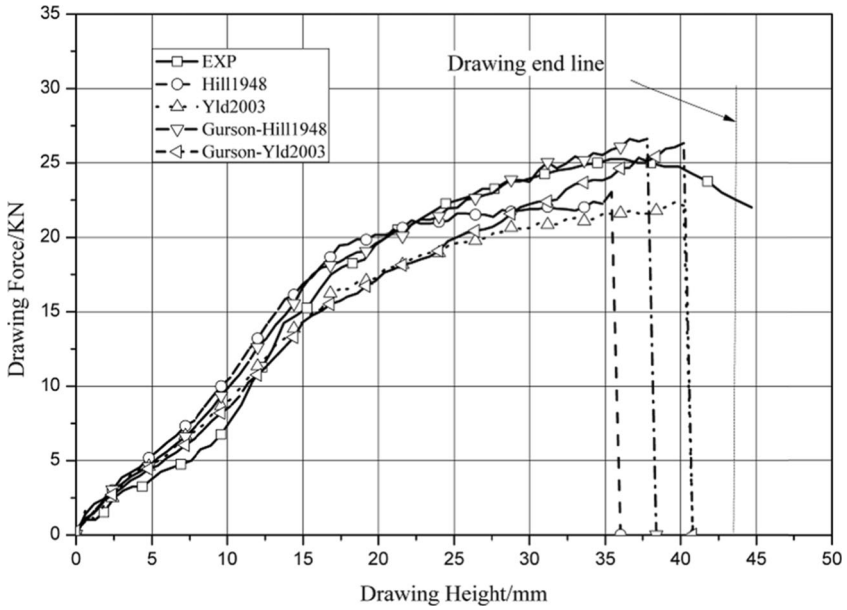

Fig. 14 Drawing force-drawing height with 95 mm diameter (1\4)

For the sample with a 95-mm diameter, two equivalent stresses including Mises and the constitutive equation are calibrated as shown in Fig. 13. Figure 13 shows that a larger difference between the equivalent stress is obtained from the Hill1948 and Yld2003 yield functions and from ABQUS. At the same time, the equivalent stress computed from the higher-order yield function is smaller than that of the lower-order yield function. The equivalent stress of the MSCM is smaller than that of the MCCM.

As shown in Fig. 14, the simulation results of the MSCM of Gurson-Hill1948 and Gurson-Yld2003 are better than those of the MCCM of Yld2003 and

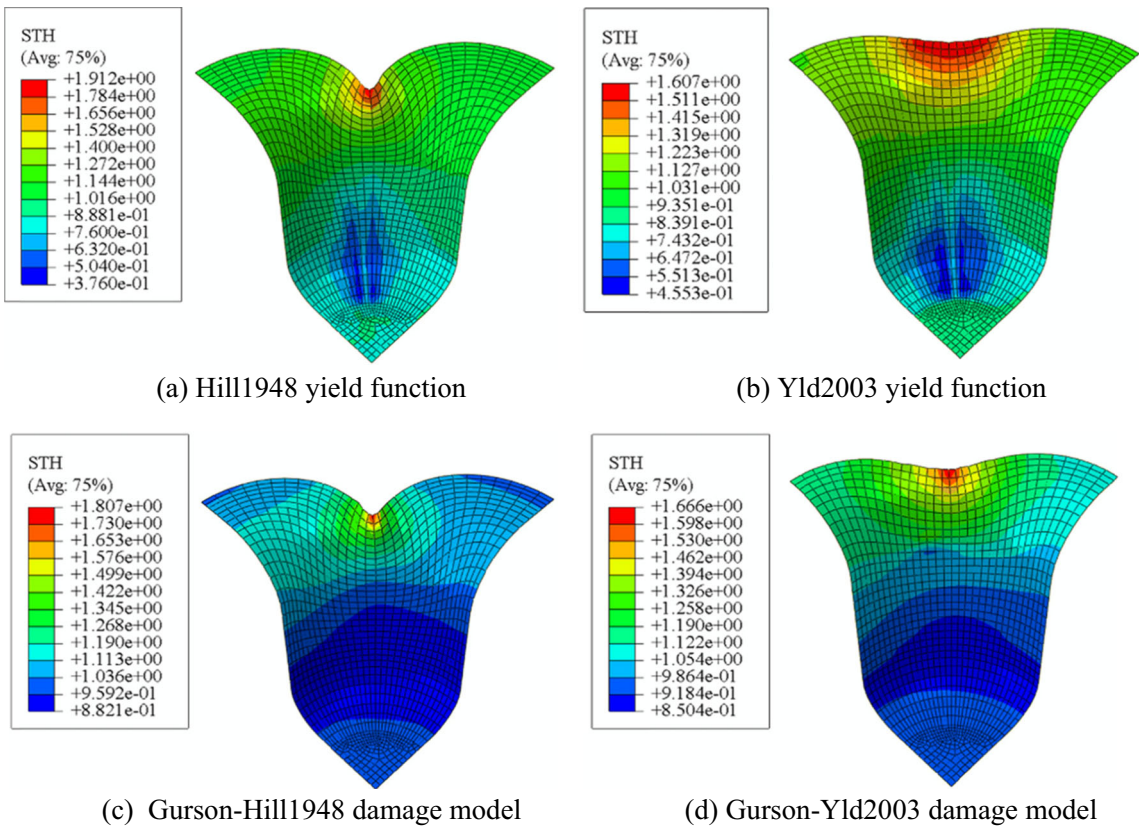

(a) Hill1948 yield function (b) Yld2003 yield function

(c) Gurson-Hill1948 damage model (d) Gurson-Yld2003 damage model

Fig. 15 The thickness distribution based on the different constitutive equations. **a** Hill1948 yield function. **b** Yld2003 yield function. **c** Gurson-Hill1948 damage model. **d** Gurson-Yld2003 damage model

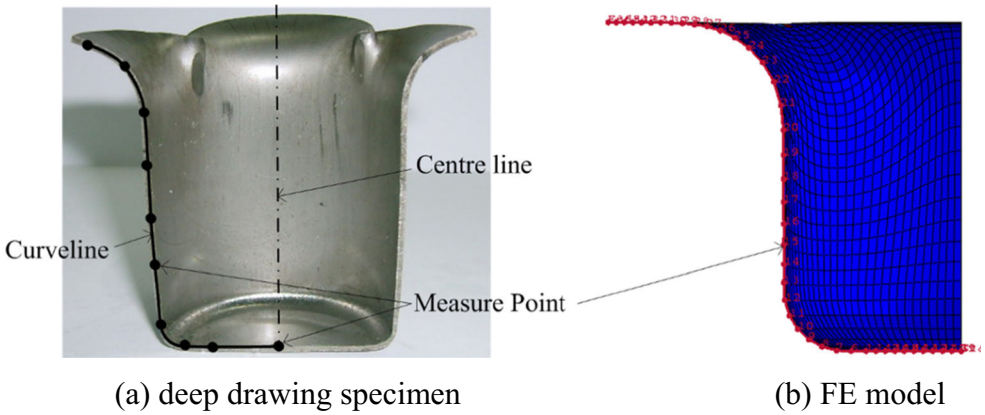

Fig. 16 Thickness testing. **a** Deep-drawing specimen. **b** FE model

Hill1948 yield functions. The predictive value of the MSCM is close to the experiment results. The preceding discussion shows that simulation results using the high-order yield function Yld2003 are in accordance with the experimental results in predicting the maximum drawing force. Therefore, the MSCM of Gurson-Hill1948 is more precise than the MCCM of the Hill1948 yield function. The advanced constitutive equation improves the precise numerical analysis.

The preceding discussion shows that normal anisotropy coefficient r changed with the increased equivalent plastic strain during the deep-drawing process. In this paper, the normal anisotropy coefficient r is fixed. The change of the normal anisotropy coefficient influences the height of the deep drawing, especially as it affects the precision of the constitutive model made by the Hill1948 yield function. The use of the MCCM and the MSCM made of the higher-order yield function decreases the influence of the normal anisotropy coefficient for drawing force and drawing height in obtaining the precise simulation results.

1. The thickness distribution

For the deep-drawing technique, thickness distribution is one of the most important parameters in the present literature. Thus, one valuable test accuracy method is to compare the thickness obtained by the simulation results with the thickness obtained by the experimental results. The thickness distribution obtained by the numerical analysis is shown in Fig. 15. To check the simulation accuracy of the thickness distribution, a test method was conducted as shown in Fig. 16. The black point expresses the test point, and the curves along these black points are used to draw the curve of the thickness distribution. In Fig. 16b, the center of the disk of the cup is considered the origin from the distance between the two adjacent points.

$$\Delta l = \sqrt{(x_{i+1}-x_i)^2 + (y_{i+1}-y_i)^2 + (z_{i+1}-z_i)^2} \tag{9}$$

Finally, the simulation and the experiment thickness obtained are shown in Fig. 17. As shown in this figure, the

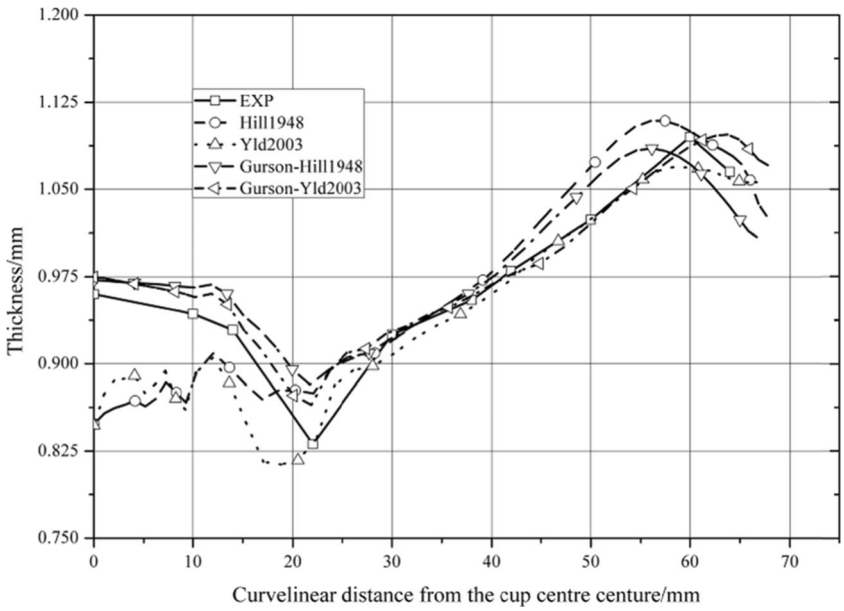

Fig. 17 The comparison between the simulation and experiment for the thickness distribution with 95 mm diameter

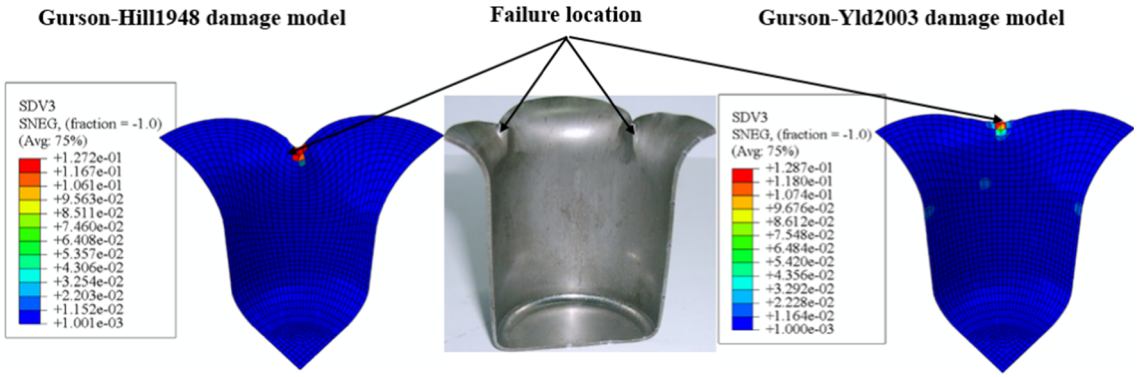

Fig. 18 The damage parameter distribution finishing the deep drawing

predictive precision of the MSCM made by the Gurson damage equation is higher than that of the MCCM, but a larger difference exists between the predictive and the test thickness values for the four constitutive equations at the corner of the punch. The result shows that the normal anisotropy coefficient r is not constant and changes with increasing deformation. In other words, the predictive results are dependent on the accuracy of the constitutive equation.

2. The damage parameter distribution

The damage parameter distribution is discussed first as shown in Fig. 18 because checking the distribution is difficult. A comparison of Figs. 13 and 18 shows that the damage parameter distribution is dependent on the equivalent strain distribution. The red region in Fig. 18 indicates a serious wrinkling region for the experimental sample. Figure 18 does not indicate the realized damage parameter distribution according to Fig. 17, and the damage parameter distribution is shown in Fig. 19.

3. The influence of the friction coefficient

In metal forming, especially in the deep-drawing process, the reduction of the friction between tool and sheet is an important task. Brosius and Mousavi [27] proposed that the deep-drawing process is an important way to save resources in the current industry. A method was presented to eliminate lubrication in the deep-drawing process by means of a new macro-structured tool design. Although the contact conditions between the tool and sheet material influences the coefficient of friction in forming processes, the coefficient of friction is often treated as a constant Coulomb friction coefficient in FE simulation.

Some studies show that the friction force between the sheet and the die and the blank prevents the finishing of the deep-drawing process. In this paper, the decrease in hydraulic pressure proved the influence of friction force. To explore the influence of friction force, this paper assumes that the friction coefficient between the sheet

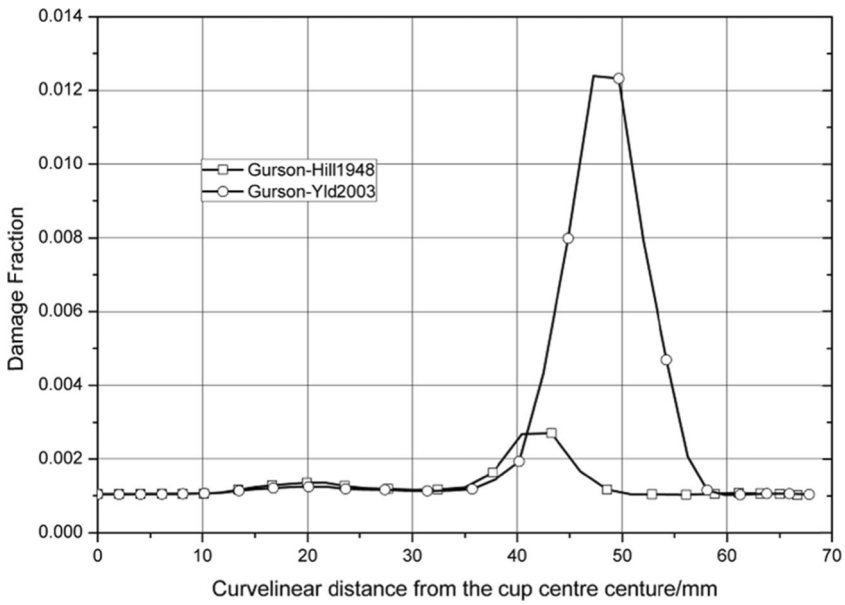

Fig. 19 The damage parameter distribution along with the curve of Fig. 16b

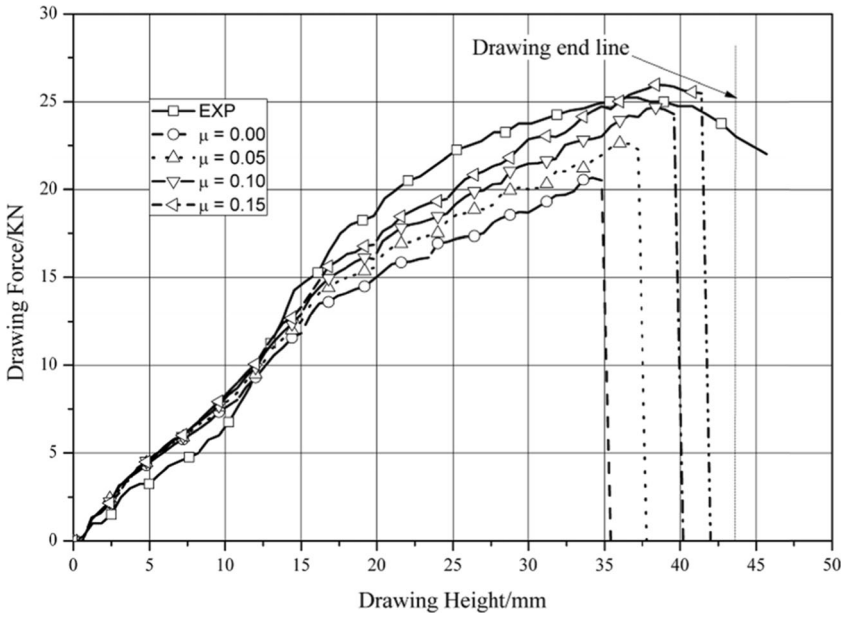

Fig. 20 The influence of the friction coefficient

and the die and the blank holder is equal to 0, 0.05, 0.10, and 0.15, respectively. At the same time, the Gurson-Yld2003 damage model is used. The deep-drawing–force-drawing heights are shown in Fig. 20. As shown in this figure, the friction coefficient has a significant influence on the drawing height and force. The friction coefficient is close to the friction coefficient between the sheet and the die.

The preceding analysis results show that the MSCM using the normal anisotropy Gurson damage equation obtains better numerical analysis accuracy. In deep drawing, the process window is limited by the occurrence of wrinkles and bottom cracks. Elimination of lubrication increases friction forces, and thus deep drawing is increased. In the future, selecting a suitable lubrication to improve deep-drawing quality is an important task.

4 Conclusions

The macroscopic constitutive model and the mesoscopic constitutive model are used to describe the deep-drawing process. A big difference shows that the mesoscopic constitutive model cannot only describe the force-displacement curve but also describe the failure phenomenon during the deep-drawing process. At the same time, an optimization method of the calibration of damage parameters was also proposed. Based on the preceding findings, the following conclusions are obtained:

1. Based on an 08Al sheet with 1-mm thickness, the mechanical performance of this specimen in different rolled directions is tested to check the anisotropy of materials. The normal anisotropy yield function and isotropy are obtained. These parameters proved that an obvious difference exists when the Hill1948 yield function was used to predict the normal anisotropy of material; the Yld2003 yield function describes the initial yield stress and the normal anisotropy coefficient. The yield equation locus using the Yld2003 and the Hill1948 yield functions show that shear stress σ_{12} has a great influence on the yield locus.
2. The damage models of the Hill1948 and Yld2003 equations and extended Gurson-Hill1948 and Gurson-Yld2003 damage models are built. The ABAQUS/Explicit user's subroutine explores the constitutive equation of the 08Al sheet. The orthogonal analysis was used to reduce the simulation times and to study the simulation results using the scientific method. This method obtains the damage parameters of the Gurson-Hill1948 and Gurson-Yld2003 by comparing the force and displacement change. Furthermore, the MSCM cannot only describe the failure location but also the sudden drawing decline, whereas the MCCM cannot.
3. The accuracy of the simulation of the deep-drawing process is explored. Comparing the simulation results with the experimental results, we discussed the sample with a 95-mm diameter. The MCCM is built by the higher-yield function Yld2003 and the MSCM based on the anisotropy of Gurson damage predicted several technique parameters. At the same time, the different friction coefficients explored the influence of the simulation results, showing that accuracy is improved when the friction coefficient is 0.1 to 0.15.

Acknowledgements This research work is financially supported by the National Natural Science Foundation of China (grant no. 51305333).

References

1. Hill R (1948) A theory of the yielding and plastic flow of anisotropy metals. P Roy Soc Lond A Mat 193:281–297
2. Barlat F, Brem JC, Yoon JW (2003) Plane stress yield function for aluminum alloy sheets—part 1: theory. Int J Plastic. 19(9):937–963
3. Hill R (1979) Theoretical plasticity of textured aggregates. Math Proc Cambridge 85:179–191
4. Hill R (1993) A user-friendly theory of orthotropic plasticity in sheet metals. Int J Mech Sci 35(1):19–25
5. Barlat F, Lian K (1989) Plastic behavior and stretchability of sheet metals. Part I: a yield function for orthotropic sheets under plane stress conditions. Int J Plastic. 5(1):51–56
6. Aretz H (2005) A non-quadratic plane stress yield function for orthotropic sheet metals. J Mater Process Technol 168(1):1–6
7. Hosford WF (1972) A generalized isotropic yield criterion [J]. Journal of Applied Mechanics of ASME 39:607–609
8. Lin, J, 2010. Study on theory and key technologies of numerical simulation for hydro-mechanical deep drawing process. Dissertation, Xi'an Jiaotong University.
9. Shang HX, Mohanram A, Olevsky E, Bordia RK (2016) Evolution of anisotropy in hierarchical porous ceramics during sinter-forging. J Eur Ceram Soc 36(12):2937–2945
10. Xue X, Liao J, Vincze G, Sousa J, Barlat F, Gracio J (2016) Modelling and sensitivity analysis of twist springback in deep drawing of dual-phase steel. Mater Des 90(15):204–217
11. Bandyopadhyay K, Panda SK, Saha P, Padmanabham G (2015) Limiting drawing ratio and deep drawing behavior of dual phase steel tailor welded blanks: FE simulation and experimental validation. J Mater Process Technol 217:48–64
12. Taherizadeh A, Green DE, Yoon JW (2011) Evaluation of advanced anisotropy models with mixed hardening evaluation of advanced anisotropy models with mixed hardening for general associated and non-associated flow metal plasticity. Int J Plastic 27(11):1781–1802
13. Barlat F, Lege DJ, Brem TC (1991) A six-component yield function for anisotropy materials. Int J Plast 9:693–712
14. Safaei M, Zang SL, Lee MG, Lee MG, Waele WD (2013) Evaluation of anisotropy constitutive models: mixed anisotropy hardening and non-associated flow rule approach. Int J Mech Sci 73:53–68
15. Moayyedian F, Kadkhodayan M (2015) Combination of modified Yld2000-2d and Yld2000-2d in anisotropy pressure dependent sheet metals. Lat Am J Solids Stru 12(1):92–114
16. McClintock FA (1968) A criterion for ductile fracture by the growth of holes. J Appl Mech 35(2):363–371
17. Rousselier G (1987) Ductile fracture models and their potential in local approach of fracture. Nucl Eng Des 105(1):97–111
18. Tvergaard V (1981) Influence of voids on shear band instabilities under plane strain conditions. Int J fracture 17:389–470
19. Guo JH, Zhao SD, Murakami R-i, Zang SL (2013) Experimental and numerical investigation for ductile fracture of Al-alloy 5052 using modified Rousselier model. Comput Mater Sci 71:115–123
20. Xu F, Zhao SD, Han XL (2014) Using of a modified Gurson model for the failure behavior of the clinched joint on Al6061 sheet. Fatig Fract Eng Mater Struct 37:335–348
21. Malte W, Eric L, Marek H, Jens-Pete M, Soren O (2015) Explicit FEM analysis of the deep drawing of paperboard. Mech Mater 89: 202–215
22. Lin J, Zhao SD, Zhang ZY, Wang ZW (2009) Deep drawing using a novel hydro-mechanical tooling. Int J Mach Tool Manu 49(1):73–80
23. Lin J, Chan LC, Wang L (2010) Prediction of forming limit diagrams based on shear failure criterion. Int J Solids Struct 47(21): 2855–2865
24. Wen T, Wang H, Yang C, Liu LT (2014) On a reshaping method of clinched joints to reduce the protrusion height. Int J Adv Manuf Technol 71(9–12):1709–1715
25. Karupannasamy DK, Hol J, De Rooij MB, Meinders T, Schipper DJ (2014) A friction model for loading and reloading effects in deep drawing processes. Wear 318(1–2):27–39
26. Zhang SH, Jensen MR, Danckerta J, Nielsen KB, Kang DC, Lang LH (2000) Analysis of the hydro-mechanical deep drawing of cylindrical cups. J Mater Process Technol 103(3):367–373
27. Brosius A, Mousavi A (2016) Lubricant free deep drawing process by macro structured tools. CIRP Ann-Manuf Techn 65(1):253–256